



**HAL**  
open science

## Application of particle filters to regional-scale wildfire spread

W. B. Da Silva, M. C. Rochoux, H. R. B. Orlande, M. J. Colaco, Olivier Fudym, Mouna El-Hafi, B. Cuenot, S. Ricci

► **To cite this version:**

W. B. Da Silva, M. C. Rochoux, H. R. B. Orlande, M. J. Colaco, Olivier Fudym, et al.. Application of particle filters to regional-scale wildfire spread. *High Temperatures-High Pressures*, 2014, 43 (6), p.415-440. hal-01625026

**HAL Id: hal-01625026**

**<https://hal.science/hal-01625026>**

Submitted on 14 Nov 2019

**HAL** is a multi-disciplinary open access archive for the deposit and dissemination of scientific research documents, whether they are published or not. The documents may come from teaching and research institutions in France or abroad, or from public or private research centers.

L'archive ouverte pluridisciplinaire **HAL**, est destinée au dépôt et à la diffusion de documents scientifiques de niveau recherche, publiés ou non, émanant des établissements d'enseignement et de recherche français ou étrangers, des laboratoires publics ou privés.

# APPLICATION OF PARTICLE FILTERS TO REGIONAL-SCALE WILDFIRE SPREAD

## **W. B. da Silva**

*Department of Mechanical Engineering, COPPE,  
Federal University of Rio de Janeiro, UFRJ, Cid.  
Universitaria, Cx. Postal: 68503 Rio de Janeiro, RJ,  
21941-972, Brazil, [wellingtonuff@yahoo.com.br](mailto:wellingtonuff@yahoo.com.br)  
Université de Toulouse ; Mines Albi ; CNRS; Centre  
RAPSODEE, Campus Jarlard, F-81013 Albi cedex 09,  
France*

## **M. C. Rochoux**

*CERFACS; SUC/CNRS URA-1875, 42 Ave. G.  
Coriolis, F-31057 Toulouse cedex 01, France.  
Ecole Centrale Paris ; CNRS UPR-288, Grande voie  
des vignes, F-92295 Châtenay-Malabry cedex,  
France,  
[melanie.rochoux@graduates.centraliens.net](mailto:melanie.rochoux@graduates.centraliens.net)*

## **H. R. B. Orlande \***

*Department of Mechanical Engineering,  
Politécnica/COPPE, Federal University of Rio de  
Janeiro, UFRJ, Cid. Universitaria, Cx. Postal:  
68503 Rio de Janeiro, RJ, 21941-972, Brazil,  
[helcio@mecanica.coppe.ufrj.br](mailto:helcio@mecanica.coppe.ufrj.br)*

## **M. J. Colaço**

*Department of Mechanical Engineering,  
Politécnica/COPPE, Federal University of Rio de  
Janeiro, UFRJ, Cid. Universitaria, Cx. Postal: 68503  
Rio de Janeiro, RJ, 21941-972, Brazil, [colaco@ufrj.br](mailto:colaco@ufrj.br)*

## **O. Fudym**

*Université de Toulouse ; Mines Albi ; CNRS; Centre  
RAPSODEE, Campus Jarlard, F-81013 Albi  
cedex 09, France, [olivier.fudym@mines-albi.fr](mailto:olivier.fudym@mines-albi.fr)*

## **M. El Hafi**

*Université de Toulouse ; Mines Albi ; CNRS; Centre  
RAPSODEE, Campus Jarlard, F-81013 Albi cedex 09,  
France, [elhafi.meh@gmail.com](mailto:elhafi.meh@gmail.com)*

## **B. Cuenot**

*CERFACS, 42 Ave. G. Coriolis, F-31057 Toulouse  
cedex 01, France, [benedicte.cuenot@cerfacs.fr](mailto:benedicte.cuenot@cerfacs.fr)*

## **S. Ricci**

*CERFACS ; SUC/CNRS URA-1875, 42 Ave. G.  
Coriolis, F-31057 Toulouse cedex 01, France,  
[sophie.ricci@cerfacs.fr](mailto:sophie.ricci@cerfacs.fr)*

\* Corresponding author



## ABSTRACT

This paper demonstrates the capability of particle filters for sequentially improving the simulation and forecast of wildfire propagation as new fire front observations become available. Particle filters, also called Sequential Monte Carlo (SMC) methods, fit into the domain of inverse modeling procedures, where measurements are incorporated (assimilated) into a computational model so as to formulate some feedback information on the uncertain model state variables and/or parameters, through representations of their probability density functions (PDF). Based on a simple sampling importance distribution and resampling techniques, particle filters combine Monte Carlo samplings with sequential Bayesian filtering problems. This study compares the performance of the Sampling Importance Resampling (SIR) and of the Auxiliary Sampling Importance Resampling (ASIR) filters for the sequential estimation of a progress variable and of vegetation parameters of the Rate Of fire Spread (ROS) model, which are all treated as state variables. They are applied to a real-world case corresponding to a reduced-scale controlled grassland fire experiment for validation; results indicate that both the SIR and the ASIR filters are able to accurately track the observed fire fronts, with a moderate computational cost. Particle filters show, therefore, their good ability to predict the propagation of controlled fires and to significantly increase fire simulation accuracy. While still at an early stage of development, this data-driven strategy is quite promising for regional-scale wildfire spread forecasting.

**KEYWORDS:** Inverse problem, Particle filters, Importance sampling, Wildfire spread.

## NOMENCLATURE

ASIR - *Auxiliary Sampling Importance Resampling*

$c$  – *Progress variable (unit: dimensionless)*

$\mathbf{c}$  – *Vector incorporating the distribution of the progress variable  $c$  for the grid points where Equation (2) is solved for each sample particle*

CPU – *Central Processing Unit*

$d$  – *Cumulative sum of weights*

$d_w$  – *Wind velocity direction (unit: °)*

EKF – *Extended Kalman Filter*

$\mathbf{f}, \mathbf{h}$  – *Functions representing the evolution and observation models*

$I_{99\%}$  - *99% - confidence interval*

MC - *Monte Carlo*

$M_f$  – *Fuel moisture content (unit: dimensionless)*

$m_w$  – *Wind velocity magnitude (unit: m/s)*

$N$  – *Number of particles*

$\mathbf{n}$  - *Normal direction to the isolines of the progress variable  $c$*

$n$  - *Number of control parameters*

$P$  – *Function modeling the rate of spread as a function of the local properties (unit: 1/s)*

$p$  - *Number of assimilated measurements*

PDF – *Probability Density Function*

$q$  - *Importance probability density*

$R$  – *Random number following a normal distribution*

RMS - *Root Mean Square*

ROS - *Rate Of Spread*

SMC - *Sequential Monte Carlo*

SIR - *Sampling Importance Resampling*

SIS - *Sequential Importance Sampling*

$t$  – *Time (unit: s)*

$u$  - Random number with uniform distribution

$\mathbf{u}_w$  - Wind velocity projected along the normal direction to the front (unit: m/s)

$\mathbf{v}$  - Modeling uncertainty vector

$\mathbf{W}$  - Observation error covariance matrix

$w$  - Particle weight

$\mathbf{x}$  - State vector

$\hat{\mathbf{x}}$  - Mean of the state vector posterior distribution

$x, y$  - Coordinates over the computational domain

$\mathbf{z}$  - Predicted measurements (simulation of observable quantities)

$\mathbf{z}^{obs}$  - Measurements (provided by remote sensing)

## Greeks

$\pi(\mathbf{x}|\mathbf{z})$  - Conditional probability density of  $\mathbf{x}$  when  $\mathbf{z}$  is given

$\Gamma$  - Rate of fire spread (unit: m/s)

$\delta$  - Fuel layer thickness (unit: m)

$\boldsymbol{\varepsilon}$  - Measurement uncertainty vector (unit: m)

$\Sigma$  - Fuel particle surface-to-volume ratio (unit: 1/m)

$\sigma_{\mathbf{x}}$  - Error standard deviation of the state vector

$\pi$  - Probability density

$\mu$  - Point estimate for transition PDF characterization

## Subscripts and Superscripts

$k$  - Time counter

$f$  - Fire front (index for the progress variable isoline  $c_f = 0.5$ )

$i, j$  - Particle index

$o$  - Observations

## 1. INTRODUCTION

Because wildfire spread is a complex multi-physics/multi-scale problem, our ability to predict their behavior at large regional scales (i.e., at scales ranging from a few tens of meters up to several kilometers) remains limited [1]. The propagation speed of wildfires, also called the Rate Of Spread (ROS), is modeled in current wildfire spread simulators as a semi-empirical function of a reduced number of parameters that locally characterize the vegetation properties, the weather conditions and the terrain topography [2,3]. In such simulators, the wildfire spread is described as a front propagating towards the unburnt vegetation (fuel) at the ROS that is relevant to the local conditions, using a standard level-set or Lagrangian front-tracking technique. The input model parameters are not easily measurable and are therefore embedded with significant levels of uncertainties. For the wildfire spread simulation to be predictive and compatible with operational applications, these uncertainties need to be quantified and reduced. For this purpose, an inverse modeling approach, based on particle filters for the solution of a state estimation problem, is proposed in this paper.

State estimation problems consist in using the available measurements together with prior knowledge about the physical phenomena and the associated uncertainties, in order to sequentially produce more accurate estimates of the dynamic variables of interest. Such problems can be solved using the Bayesian filtering approach [4-8]. This methodology formally involves the Bayes' theorem and aims at minimizing the amount of uncertainty in the quantities of interest, as new information become available. Recent progress made in airborne remote sensing provides new ways to monitor real-time fire front positions; Bayesian filtering appears as an efficient framework to formulate some feedback information on the fire dynamics and to produce improved forecasts of the wildfire propagation.

The most widely known Bayesian filter method is the Kalman filter [4-7]. However, this filter is limited to linear models and Gaussian assumptions regarding the statistical description of errors. While extensions of the Kalman filter are widely used for less restrictive cases by using linearization techniques, particle filters have been specifically developed to deal with non-linear models and non-Gaussian errors [8,9]. Particle filters were introduced in the 1950s with a Sequential Importance Sampling (SIS) technique, which used recursive Bayesian filters together with Monte Carlo (MC)

simulations. The key idea was to describe the Probability Density Functions (PDF) of the state variables as a set of random particles (prior); each particle was then associated with a weight that was calculated using the measurements along with their uncertainties; the values of the particles and their associated weights allowed a more accurate PDF (posterior) to be retrieved. To avoid the degeneracy problem (i.e., to avoid that only a few particles participate effectively in the filtering process), Gordon et al. [10] added a resampling approach into the SIS filter. Resampling can be either applied if the number of effective particles falls below a specified threshold number, or at every step in a technique known as the Sampling Importance Resampling (SIR) filter. A large number of recent studies have highlighted the performance of the SIR filter over a wide range of applications [11]. Despite these applications, the SIR filter remains computationally intensive, as a large number of particles is required to obtain a complete and accurate statistical description of the state variables. In order to overcome these difficulties, Pitt and Shephard [12] introduced the auxiliary particle filters, whose main idea was to improve the prior information by using an additional set of particles (called auxiliary particles), so as to reduce the computational cost without degrading the accuracy of the result. In this perspective, Silva et al. [13] applied the Auxiliary Sampling Importance Resampling (ASIR) filter to solve a non-linear solidification problem, where simulated temperature measurements were used to estimate a transient line heat sink as well as the solidification front. Colaço et al. [14] compared the performance of the SIR and ASIR filters in the estimation of the heat flux applied to a square cavity in a natural convection problem; this study showed excellent estimates for the time variation of the unknown quantity. Hamilton et al. [15] applied the SIR filter to estimate the heat transfer coefficient between the product gases and the walls of an internal combustion engine chamber. The algorithm was able to recover the unknown function with small Central Processing Unit (CPU) times, even for very high uncertainties in the initial state. It was also demonstrated that the variance of the error between the mean solution and its true value decreases with the number of particles used in the filter. In other works, the sequential propagation of modeling errors was also studied to improve the choice of the particles at the next observation time (i.e., at the next assimilation cycle), in particular in the case of combined parameter-state estimation [8,16].

The application of inverse methods in the context of fire modeling has been considered only recently [17-20]. Gu [18] applied the SIR algorithm to synthetic cases of wildfire spread, in order to estimate average wind magnitude or wind direction of a semi-empirical model in the fire area using ground-based temperature sensor data. More recently, Rochoux et al. [19] demonstrated the applicability and performance of an Extended Kalman filter (EKF) algorithm for estimating input parameters of a Rothermel-based ROS model [2] using reconstructed measurements of the fire front locations in a real controlled fire experiment and a level-set front-tracking simulator called FIREFLY. Unfortunately, the predictions obtained with the EKF are believed to be of limited value for more realistic cases, like those involving regional-scale fires strongly coupled to atmospheric dynamics, with heterogeneous vegetation properties as well as non-constant wind velocity that enhance non-linearities between environmental conditions and the fire propagation. A recent work by Xue et al [20] presented the application of the SIR algorithm of the particle filter for the prediction of wildfire spread. However, this work was based on temperature measurements spread through the region of interest and only involved (synthetic) simulated data.

The objective of this paper is to address the challenges specific to the development of a robust inverse modeling approach for realistic wildfire spread. To better take into account the underlying model non-linearities and thus to provide more accurate posterior distributions of the state variables, we propose here a particle filter strategy based on the assimilation of the time-evolving fire front locations and the front-tracking fire spread simulator FIREFLY, such as in references [19,21]. Both the SIR and the ASIR algorithms of the particle filter are implemented and compared, when applied to actual measured data obtained from a controlled experiment. While limited to a reduced-scale fire at this early stage of development, this validation test is fundamental for providing valuable information, insight and understanding on the performance of the data-driven wildfire spread model.

The paper is organized as follows: Section 2 presents the FIREFLY simulation capability of fire spread (also called the forward or direct model); the SIR and ASIR particle filter algorithms used for the solution of the state estimation problem are introduced in Section 3; and results are presented in Section 4 for a validation test based on comparisons with a small-scale (4 m x 4 m) controlled grassland fire experiment.

## 2. THE FIRE PROPAGATION MODEL (THE FORWARD MODEL)

The propagation of wildfires results from complex interactions between pyrolysis, combustion, heat transfer and flow dynamics, as well as atmospheric dynamics and chemistry, among other phenomena. These interactions occur over a wide range of scales: vegetation scales that characterize the biomass fuel; topographical scales that characterize the terrain and vegetation boundary layer; and meteorological micro-/meso-scales that characterize atmospheric conditions. As in current operational wildfire spread models [3], we adopt in this study a regional-scale perspective and simulate a wildfire as a thin flame zone (i.e., as a front) that self-propagates normal to itself towards the unburnt vegetation. In this representation, the main quantity of interest is the ROS, that is the local propagation speed of the front. Note that the present study is limited to flat terrains and problems with complex topography are outside its scope.

### 2.1. SUBMODEL FOR THE RATE OF SPREAD

In this approach based on Rothermel's model [2], the ROS is formulated as a semi-empirical function of a reduced number of parameters that locally characterize the vegetation (fuel) properties, the weather conditions and the terrain topography. The local ROS, denoted by  $\Gamma$  [m/s], can be written as

$$\Gamma \equiv \Gamma(x, y, t) = P\left(M_f, \Sigma, \mathbf{u}_w(x, y, t), \dots\right) \delta(x, y), \quad (1)$$

where  $\delta$  [m] is the fuel depth (*e.g.*, the vegetation layer thickness) and  $P$  [1/s] is a function of the fuel moisture content  $M_f$  (mass of water divided by mass of dry fuel), the fuel particle surface-to-volume ratio  $\Sigma$  [1/m], and the wind velocity (at mid-flame height)  $\mathbf{u}_w$  [m/s]. In this paper,  $\Sigma$ ,  $M_f$  and  $\delta$  are treated as spatially-uniform parameters. Note that  $\mathbf{u}_w$  is spatially-distributed along the fire front evolving on the two-dimensional horizontal plane  $(x, y)$ . This variable results from the projection of the wind velocity vector (assumed spatially-uniform over the two-dimensional horizontal plane  $(x, y)$  and defined by the wind velocity magnitude and direction, denoted by  $m_w$  and  $d_w$ , respectively) along the normal direction to the contour lines of the progress variable denoted by  $\mathbf{n} = \mathbf{n}(x, y, t)$ .  $\mathbf{u}_w$  is also time-

varying due to the anisotropy in the wind-aided wildfire spread and to the subsequent changing shape of the fire front. Thus,  $\mathbf{u}_w = \mathbf{u}_w(x,y,t)$ .

## 2.2. LEVEL-SET FRONT-TRACKING TECHNIQUE

In the FIREFLY simulation capability, the propagation of the fire front at the ROS given by Equation (1) is simulated using a standard level-set front-tracking technique [19]. As in the premixed combustion literature [22], a progress variable, denoted  $c$  and also referred to as the level-set function, is introduced as a flame marker:  $c = 0$  in the unburnt vegetation,  $c = 1$  in the burnt vegetation; and the flame front is identified by the two-dimensional contour line  $c_f = 0.5$ , as shown in Figure 1.

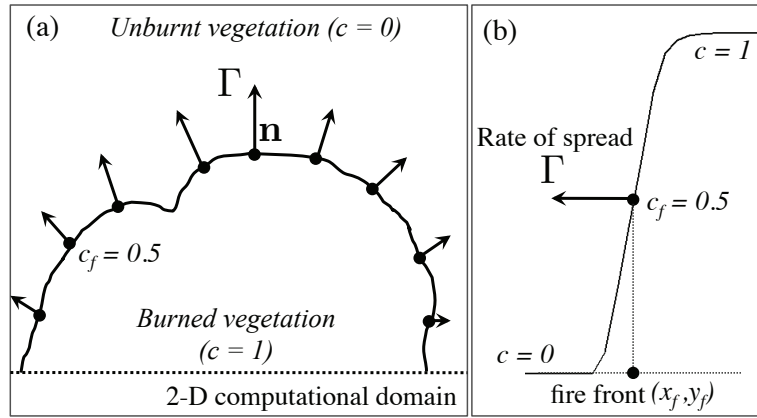


Figure 1: Schematic of the fire propagation model: (a) 2-D surface fire spread at the ROS  $\Gamma$  along the normal direction  $\mathbf{n}$  to the front (b) Profile of the progress variable  $c$  throughout  $c_f = 0.5$ .

The locations of the fire front are reconstructed using the two following steps: 1) a level-set based solver for the progress variable  $c = c(x,y,t)$ , and 2) an isoline algorithm for the reconstruction of the discretized fire front  $(x_i, y_i)$  with  $i \leq 1 \leq N_f$ .

### 2.2.1. PROPAGATION EQUATION

The spatio-temporal evolution of the progress variable  $c = c(x,y,t)$  is calculated as a solution of the following propagation equation using the ROS model due to Rothermel in Equation (1):

$$\frac{\partial c}{\partial t} = \Gamma |\nabla c|, \quad (2)$$

with  $\Gamma$  being the ROS [m/s] along the normal direction  $\mathbf{n} = -\nabla c / |\nabla c|$  to the contour lines of the progress variable  $c$ . Equation (2) is solved by using a second-order Runge-Kutta scheme for time-integration and a second-order total variation diminishing scheme with a Superbee slope limiter for spatial discretization, following choices made by Rehm and McDermott [23].

### 2.2.2. RECONSTRUCTION OF THE DISCRETIZED FIRE FRONT

The instantaneous position of the fire front  $(x_i, y_i)$  is extracted using a simple isoline algorithm, verifying  $c(x_i, y_i, t) = c_f$  with  $c_f = 0.5$  and  $i \leq 1 \leq N_f$  ( $N_f$  being the total number of simulated markers). First, this algorithm extracts the contour line  $c_f = 0.5$  from the two-dimensional progress variable  $c$  with respect to the computational grid resolution on the horizontal plane  $(x, y)$  in FIREFLY. Second, this algorithm discretizes the contour line  $c_f = 0.5$  with a fixed number ( $N_f$ ) of equally-spaced markers. Further technical details on the isoline algorithm are provided in reference [21].

### 2.2.3. FORWARD MODEL OPERATOR

Following these two steps, the outputs of the FIREFLY model can be represented as a composition of the integration of Equation (2) that provides the state of the spatially-varying progress variable  $c$  at a given time, with the isoline algorithm which identifies the discretized contour line  $c_f = 0.5$  as the front marker locations  $(x_i, y_i)$  with  $i \leq 1 \leq N_f$ . This composition of operations that leads to the location of the front markers (corresponding to a fine-grained discretization of the simulated fire front) is referred to as the forward model operator; this operator takes as inputs the initial condition of the progress variable  $c$  as well as the input parameters of the Rothermel-based ROS model  $\Gamma$ .

## 3. THE INVERSE PROBLEM

Particle filters [8-15] provide an attractive framework for integrating fire sensor observations with computational models, accounting for both observation and modeling errors (these errors are not

necessarily assumed to be additive or to follow a Gaussian PDF), and thus for providing accurate estimates of poorly known parameters [24] as well as improved predictions of fire spread dynamics.

### 3.1. PRINCIPLES OF THE BAYESIAN SOLUTION FOR AN INVERSE PROBLEM

Particle filters require the definition of the following mathematical quantities: 1) the state vector that describes the variables to be estimated/controlled in the particle filter algorithm, and 2) the observation operator that maps the state space onto the observation space.

#### 3.1.1. STATE VECTOR

The vector  $\mathbf{x}_k \in \mathbf{R}^n$  is called the state vector and contains the  $n$  model variables to be dynamically estimated. This vector advances in time in accordance with the evolution model of the parameters defined as follows:

$$\mathbf{x}_k = \mathbf{f}_k(\mathbf{x}_{k-1}, \mathbf{v}_k), \quad (3)$$

where  $\mathbf{f}_k$  can be a non-linear function of the state vector  $\mathbf{x}_{k-1}$  and of the uncertainty vector  $\mathbf{v}_{k-1} \in \mathbf{R}^n$ ; the subscript  $k$  refers to the time  $t_k$ . In this study, the vector  $\mathbf{v}_k$  is modeled with random variables following a Gaussian PDF. The objective here is to accurately estimate the fire front location together with two fuel parameters, namely, the fuel moisture content,  $M_f$ , and the fuel particle surface-area-to-volume ratio,  $\Sigma$ . Thus, the state vector is given by  $\mathbf{x} = (\mathbf{c}, M_f, \Sigma)^T$ , where the vector  $\mathbf{c}$  includes the spatial distribution of the progress variable  $c$  at the grid points at which Equation (2) is solved for each sample particle.

As there is no explicit formulation of the evolution of the control parameters between two successive observation times, a random walk model is used as the evolution model for them. Note that this random walk model is such that the evolution function is identity and to which Gaussian noise (with zero mean and given variance) is added (see Section 4 for further details specific to the wildfire spread application).

### 3.1.2. OBSERVATION OPERATOR

The observation vector  $\mathbf{z}_k^{obs} \in \mathbf{R}^p$  contains the  $p$  measurements of the fire front locations at the assimilation time  $t_k$ . To estimate the model deviation from the measurements  $\mathbf{z}_k^{obs}$ , an observation model is introduced through the general, possibly non-linear, function  $\mathbf{h}_k$ , which describes the dependence between the state variables  $\mathbf{x}_k$  and the simulated fire front locations  $\mathbf{z}_k$  (predicted measurements) designated as:

$$\mathbf{z}_k = \mathbf{h}_k(\mathbf{x}_k, \boldsymbol{\varepsilon}_k) \quad (4)$$

where  $\mathbf{z}_k \in \mathbf{R}^p$  includes here the  $(x_i^o, y_i^o)$ -coordinates of the  $p$  discrete front locations at time  $t_k$ , and the vector  $\boldsymbol{\varepsilon}_k \in \mathbf{R}^p$  represents the measurement uncertainty vector. The vector  $\boldsymbol{\varepsilon}_k$  is also modeled with random variables following a Gaussian PDF. Note that  $p = 2 N_f^o$  ( $N_f^o$  is the number of markers along the observed front, each marker being associated with a pair of coordinates  $(x_i^o, y_i^o)$ , with  $i \leq 1 \leq N_f^o$ ).

In this study, the observation operator represents the calculation of a distance between the fine-grained discretization of the simulated fire front and the discretized observation fire front. Stated differently, the observation markers  $(x_i^o, y_i^o)$  with  $i \leq 1 \leq N_f^o$  are mapped onto the simulated fire front in order to determine their model counterparts  $(x_i, y_i)$  with  $i \leq 1 \leq N_f$ . For this purpose, the observation operator pairs a subset of  $N_f$ -markers along the fine-grained discretization of the simulated fire front with the  $N_f^o$  markers along the coarse-grained discretization of the observed fire front, associating each marker of the observed fire front with its closest neighbor along the simulated fire front (see Figure 2).

The observation function  $\mathbf{h}_k$  may be defined in several ways (for instance using a projection scheme) but preliminary tests have shown that a simple treatment (taking 1 out of every  $N_f/N_f^o$  markers) provided reasonable results [21]. The number of observed front markers  $N_f^o$  is typically much lower than  $N_f$ , since FIREFLY requires a high-resolution computational grid and since observations are commonly provided with a much coarser resolution ( $N_f/N_f^o > 1$ ). One of the advantages of this mapping procedure is that it provides a local information on the discrepancies between simulated and observed fire fronts and not only a global information such as the difference in the burnt area or in the fireline perimeter. This local information is efficient at tracking the anisotropy in wildfire spread. Still,

the topology of the fire front can be complex in real-world wildfire spread cases, and/or only a section of the fire front can be observed due to the opacity of the fire-induced thermal plume or due to a limited monitoring. The performance of the mapping procedure needs therefore to be evaluated for such scenarios, where the pairing between simulated markers and observed markers becomes more challenging for complex fire front topologies. However, this issue is out of the scope of this study that aims at showing the potential of particle filters for wildfire spread forecasting; the extension of the mapping procedure to more realistic fire front topologies is one of the next challenges towards operational applications. Projection schemes reported in Ref. [21] are expected to provide a valuable answer to this issue and could be integrated to the particle filters algorithms in future works.

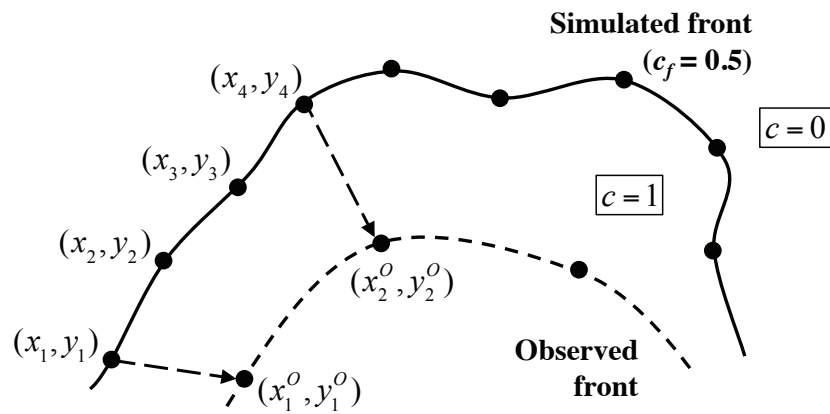


Figure 2 - Calculation of the distance between simulated and observed fire fronts, defined as the vector formed by the distances between the paired simulated and observed front markers. In this illustration,

$$N_f/N_f^o = 4.$$

### 3.1.3. BAYES' THEOREM

The formal mechanism to combine measurements and prior information on the state variables is Bayes' theorem [4-8]. Therefore, the term Bayesian is often used to describe the statistical inversion approach that is based on the following principles:

- 1) Both state vector  $\mathbf{x}_k$  and observation vector  $\mathbf{z}_k^{obs}$  are modeled as random variables;
- 2) The level of uncertainty in the realization of these random variables is described via PDF, denoted  $\pi(\mathbf{x}_k)$  and  $\pi(\mathbf{z}_k^{obs})$ , respectively;

3) The sequences of these random variables are assumed to be discrete time Markov chains, which are assumed to satisfy the following properties [4-8]:

(a) The distribution of the control vector  $\mathbf{x}_k$  at time  $t_k$  is only determined by its most recent value at time  $t_{k-1}$ , meaning that the future and past distributions of the control vector  $\mathbf{x}$  are independent, that is,

$$\pi(\mathbf{x}_k | \mathbf{x}_0, \mathbf{x}_1, \mathbf{K}, \mathbf{x}_{k-1}) = \pi(\mathbf{x}_k | \mathbf{x}_{k-1}) \quad (5)$$

(b) The sequence of observation vectors  $\mathbf{z}_k^{obs}$  ( $k = 1, 2, 3, \dots$ ) is a Markovian process with respect to the history of  $\mathbf{x}_k$ , that is,

$$\pi(\mathbf{z}_k^{obs} | \mathbf{x}_0, \mathbf{x}_1, \mathbf{K}, \mathbf{x}_k) = \pi(\mathbf{z}_k^{obs} | \mathbf{x}_k) \quad (6)$$

(c) The sequence of state vectors  $\mathbf{x}_k$  ( $k = 1, 2, 3, \dots$ ) depends on the past observations only through its own history, that is,

$$\pi(\mathbf{x}_k | \mathbf{x}_{k-1}, \mathbf{z}_1^{obs}, \mathbf{z}_2^{obs}, \mathbf{K}, \mathbf{z}_{k-1}^{obs}) = \pi(\mathbf{x}_k | \mathbf{x}_{k-1}) \quad (7)$$

4) The objective of the Bayesian inverse problem is to retrieve the posterior PDF  $\pi_{posterior}(\mathbf{x}_k)$ , i.e., the update of the prior PDF  $\pi(\mathbf{x}_k)$  characterizing the prior information available on the state variables. This update is expected to be more consistent with the measurements.

In this context, the Bayes' theorem is stated as

$$\pi_{posterior}(\mathbf{x}_k) = \pi(\mathbf{x}_k | \mathbf{z}_k^{obs}) = \frac{\pi(\mathbf{x}_k) \pi(\mathbf{z}_k^{obs} | \mathbf{x}_k)}{\pi(\mathbf{z}_k^{obs})}, \quad (8)$$

where

- $\pi(\mathbf{x}_k)$  corresponds to the prior density of the state variables;
- $\pi(\mathbf{z}_k^{obs})$  corresponds to the marginal probability density of the measurements, which plays the role of a normalizing constant;
- $\pi(\mathbf{z}_k^{obs} | \mathbf{x}_k)$  corresponds to the likelihood (i.e., the conditional probability of the measurements  $\mathbf{z}_k^{obs}$  given the state variables  $\mathbf{x}_k$ ). In this paper, the measurement errors are assumed to be additive, Gaussian, with zero mean and a covariance matrix  $\mathbf{W}$ , so that we can write:

$$\pi(\mathbf{z}_k^{obs} | \mathbf{x}_k) = (2\pi)^{-p/2} |\mathbf{W}|^{-1/2} \exp \left\{ -\frac{1}{2} [\mathbf{z}_k^{obs} - \mathbf{z}_k]^T \mathbf{W}^{-1} [\mathbf{z}_k^{obs} - \mathbf{z}_k] \right\}, \quad (9)$$

with  $\mathbf{z}_k$  are the predicted observed variables resulting from the FIREFLY simulation provided by Equation (4) (the prediction of the fire front locations at time  $t_k$  with known parameters  $\mathbf{x}_k$ ) and  $\mathbf{W}$  is diagonal, as the measurement errors are assumed to be uncorrelated.

### 3.2. THE BAYESIAN FILTERING PROBLEM

In the present study, we consider a filtering problem that aims at finding the most accurate PDF of the control vector  $\mathbf{x}_k$  given the past observations up to time  $t_k$ , that is at approximating the posterior distribution  $\pi(\mathbf{x}_k | \mathbf{z}_{1:k}^{obs})$ . The Bayesian filtering process can be divided into two steps, prediction and update, which can be generally described as follows: (i) We first choose a prior distribution of the control vector  $\pi(\mathbf{x}_0)$  over the state space at the initial time  $t = 0$ . Then, as one observation  $\mathbf{z}_l^{obs}$  is available at time  $t_l$ , we predict the distribution  $\pi(\mathbf{x}_1)$  using the Markov property of  $\mathbf{x}_1$ , see Equation (7). (ii) Using Bayes' theorem and in particular the likelihood  $\pi(\mathbf{z}_l^{obs} | \mathbf{x}_l)$ , we can then estimate the posterior PDF  $\pi_{posterior}(\mathbf{x}_1) = \pi(\mathbf{x}_1 | \mathbf{z}_l^{obs})$  using Equation (8). This algorithm can then be applied sequentially for all observation times ( $k = 1, 2, \dots, K$ ).

The Kalman filter is a widely known Bayesian filtering method; it provides the exact analytical solution of the posterior distribution when dealing with linear models and additive Gaussian noises. As a mean of addressing the difficulties encountered in non-linear problems, Monte Carlo (MC) methods based on particle filters represent the posterior PDF of the state variables by using a finite number of randomly generated model trajectories; they do not constrain *a priori* the shape of the PDF that is to be found. The statistics made on the ensemble of realizations is used to reconstruct the posterior PDF of the control parameters by using Equation (8), which is then propagated to the next observation time (by using an evolution model of the state variables).

As the number of particles becomes very large, this MC characterization becomes an equivalent representation of the posterior PDF, and the solution approaches the optimal Bayesian estimate [4-16]. In the following, some particle filters algorithms are briefly revised, as they were used in this work for estimating the wildfire ROS.

### 3.3. THE SEQUENTIAL IMPORTANCE SAMPLING (SIS) FILTER

Most particle filters rely on the Sequential Importance Sampling (SIS). This algorithm is based on the calculation of an importance density, i.e., a density that is used to build the particles instead of the exact posterior density that cannot be exactly computed. The PDF of the state vector  $\mathbf{x}$  is sampled with  $N$  particles. We consider the set of particles  $\{\mathbf{x}_{0:k}^i, i = 0, K, N\}$  associated with the normalized weights

$\{w_k^i, i = 0, K, N\}$  satisfying  $\sum_{i=1}^N w_k^i = 1$ . The posterior density at time instant  $t_k$  can be discretely

approximated by [5-10]:

$$\pi(\mathbf{x}_k | \mathbf{z}_{1:k}^{obs}) \approx \sum_{i=1}^N w_k^i \delta(\mathbf{x}_k - \mathbf{x}_k^i), \quad (10)$$

with  $\delta(\cdot)$  being the Dirac delta function and the weights computed from [9]:

$$w_k^i \propto w_{k-1}^i \frac{\pi(\mathbf{z}_k^{obs} | \mathbf{x}_k^i) \pi(\mathbf{x}_k^i | \mathbf{x}_{k-1}^i)}{q(\mathbf{x}_k^i | \mathbf{x}_{k-1}^i, \mathbf{z}_k^{obs})}, \quad (11)$$

where the importance density  $q(\mathbf{x}_k^i | \mathbf{x}_{k-1}^i, \mathbf{z}_{1:k}^{obs})$  is assumed to be a Markovian process. The optimal choice of the importance density, which minimizes the variance of the importance weights conditioned upon control parameters  $\mathbf{x}_{k-1}^i$  and measurements  $\mathbf{z}_k^{obs}$ , is given by  $q(\mathbf{x}_k^i | \mathbf{x}_{k-1}^i, \mathbf{z}_k^{obs}) = \pi(\mathbf{x}_k^i | \mathbf{x}_{k-1}^i, \mathbf{z}_k^{obs})$ .

However, for most practical problems, this optimal choice is not analytically tractable and a suboptimal importance density is taken as the transition prior, that is,  $q(\mathbf{x}_k^i | \mathbf{x}_{k-1}^i, \mathbf{z}_k^{obs}) = \pi(\mathbf{x}_k^i | \mathbf{x}_{k-1}^i)$  [9], so that

Equation (11) reduces to

$$w_k^i \propto w_{k-1}^i \pi(\mathbf{z}_k^{obs} | \mathbf{x}_k^i). \quad (12)$$

Figure 3 shows a schematic representation of the Sampling Importance Sampling (SIS) Filter. Here, the key idea is to sample the prior PDF by a large set of random particles; the forward model is integrated for each particle and thus a weight is given to each model trajectory as a function of the distance to the measurements (likelihood), see Equation (9).

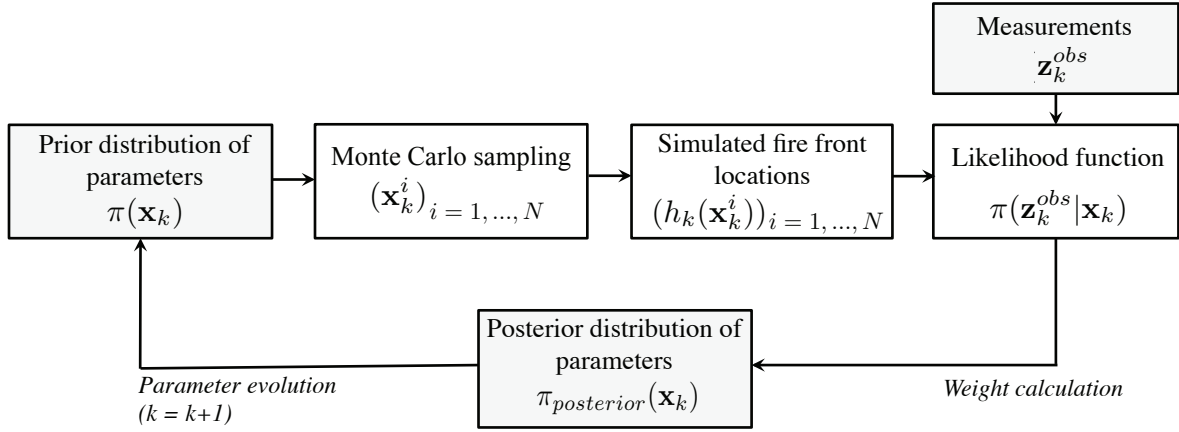


Figure 3: Schematic of the Sampling Importance Sampling (SIS) Filter.

The SIS algorithm for the time period  $[t_{k-1}, t_k]$  is summarized in Table 1.

Table 1. SIS algorithm [8,9].

STEP 1
Draw new particles $\mathbf{x}_k^i$ ( $i = 1, \dots, N$ ) from the prior density $\pi(\mathbf{x}_k   \mathbf{x}_{k-1}^i)$ and then use the likelihood density to calculate the corresponding weights $w_k^i = w_{k-1}^i \pi(\mathbf{z}_k^{obs}   \mathbf{x}_k^i)$ .
STEP 2
Compute the normalized particle weights so that $w_k^i = w_k^i / \sum_i w_k^i$ ( $i=1, \dots, N$ ).

### 3.4. THE SAMPLING IMPORTANCE RESAMPLING (SIR) FILTER

The application of the SIS particle filter might result in the degeneracy problem, meaning that after a couple of estimations all but very few particles will have negligible weights [5-10]. If this problem occurs, a large computational effort is devoted to updating particles whose contribution to the approximation of the posterior PDF is almost zero. In practice, this problem can be overcome by adding a resampling step in the SIS particle filter algorithm.

The resampling process involves a mapping of the random measures  $\{\mathbf{x}_k^i, w_k^i\}$  into  $\{\mathbf{x}_k^{i*}, 1/N\}$  with uniform weights equal to  $1/N$  (where  $N$  is the number of particles). This leads to the elimination of particles with low weights and additional sampling in the vicinity of the particles with large weights (effective particles). Resampling could be performed if the number of effective particles falls below a certain threshold number, but in the following algorithm resampling is indistinctively applied at every

time  $t_k$ . Such algorithm is called the Sampling Importance Resampling (SIR) filter [8,9] and can be summarized in the three main steps presented in Table 2. Note that in the first step the weights are given directly by the likelihood function  $\pi(\mathbf{z}_k^{obs} | \mathbf{x}_k^i)$  since the weights of the previous filtering step at time  $t_{k-1}$  (noted  $w_{k-1}^i$ ) are uniform.

Table 2. SIR algorithm [8,9].

STEP 1
Draw new particles $\mathbf{x}_k^i$ ( $i = 1, \dots, N$ ) from the prior density $\pi(\mathbf{x}_k   \mathbf{x}_{k-1}^i)$ and then use the likelihood density to calculate the corresponding weight $w_k^i = \pi(\mathbf{z}_k^{obs}   \mathbf{x}_k^i)$ .
STEP 2
Compute the normalized particle weights so that $w_k^i = w_k^i / (\sum_i w_k^i)$ ( $i=1, \dots, N$ ).
STEP 3
Resample the particles as follows: a) Construct the cumulative sum of weights (CSW) by computing $d_i = d_{i-1} + w_k^i$ for $i=1, \dots, N$ , with $d_0=0$ b) Start from $i = 1$ and draw a starting point $u_1$ from the uniform distribution $U[0,1/N]$ c) For $j = 1, \dots, N$ : i) Move along the CSW by making $u_j = u_1 + (j-1)/N$ ii) While $u_j > d_i$ make $i = i+1$ iii) Assign sample $\mathbf{x}_k^j = \mathbf{x}_k^i$ iv) Update weight $w_k^j = 1/N$ (uniform)

### 3.3. THE AUXILIARY SAMPLING IMPORTANCE RESAMPLING (ASIR) FILTER

Although the resampling step reduces the effects of the degeneracy problem, it may lead to an updated sample containing many repeated particles. Hence, despite the fact that the weights are easily computed and that the importance density can be easily sampled within the framework of the SIR algorithm, the particles may quickly suffer from a loss of diversity. This problem, known as sample impoverishment, can be severe in the case of small state evolution noise [5,8,9]. In addition, by using the SIR algorithm, the state space is explored without the information conveyed by the measurements, that is, the particles at each time are generated through the sole application of the transition prior  $\pi(\mathbf{x}_k^i | \mathbf{x}_{k-1}^i)$  (see the first step in Table 2).

With the Auxiliary Sampling Importance Resampling (ASIR) algorithm [8,9] presented in Table 3, an attempt is made to overcome these drawbacks by performing the resampling step at the

previous time  $t_{k-1}$  with the available measurements at time  $t_k$ . The resampling is based on some point estimate  $\mu_k^i$ , chosen either as the mean or as a sample of the transition density  $\pi(\mathbf{x}_k|\mathbf{x}_{k-1}^i)$ , which characterizes the evolution of the control distribution from  $t_{k-1}$  to  $t_k$ . For the sake of generality, the second approach was used in this work. If the noise of the evolution model is small,  $\pi(\mathbf{x}_k|\mathbf{x}_{k-1}^i)$  is generally well characterized by  $\mu_k^i$ , meaning that this improved prior information will lead to a more efficient filtering than the standard SIR algorithm and thus all the resulting particles will have a similar weight. In the opposite, if the noise of the parameter evolution model is large, the single point estimate  $\mu_k^i$  in the control space may not characterize well  $\pi(\mathbf{x}_k|\mathbf{x}_{k-1}^i)$  and the ASIR algorithm may not be as effective as the SIR filter. The use of such characterization  $\mu_k^i$  means that the SIR and ASIR filters are not based on the same definition of the importance density.

In general, a drawback of particle filters is related to the large computational cost due to the MC method. However, solutions exist to make particle filters affordable for more complicated physical problems. More advanced algorithms have been specifically developed to build an appropriate representation of the posterior PDF with a small number of particles and thus with a reduced computational time [8,9]. In addition, the use of surrogate models or response surfaces for the solution of the forward model appears as promising approaches for solving Bayesian filtering problems within a reasonable computational cost [25-28].

Table 3. ASIR algorithm [8,9].

STEP 1
Draw new particles $\mathbf{x}_k^i$ ( $i=1, \dots, N$ ) from the prior density $\pi(\mathbf{x}_k \mathbf{x}_{k-1}^i)$ and then calculate some characterization (for example, the mean) $\mu_k^i$ of $\mathbf{x}_k$ , given $\mathbf{x}_{k-1}^i$ . Use the likelihood density to calculate the corresponding weight $w_k^i = w_{k-1}^i \pi(\mathbf{z}_k^{obs} \mu_k^i)$
STEP 2
Normalize the particle weights so that $w_k^i = w_k^i / \sum_i w_k^i$ ( $i=1, \dots, N$ )
STEP 3
Resample the particles as follows: a) Construct the cumulative sum of weights (CSW) by computing $d_i = d_{i-1} + w_k^i$ for $i = 1, \dots, N$ , with $d_0=0$ b) Start from $i=1$ and draw a starting point $u_1$ from the uniform distribution $U[0,1/N]$ c) For $j = 1, \dots, N$ : i) Move along the CSW by making $u_j = u_1 + (j-1)/N$ ii) While $u_j > d_i$ make $i=i+1$ iii) Assign sample $\mathbf{x}_k^j = \mathbf{x}_k^i$ iv) Update weight $w_k^j = 1/N$ (uniform) v) Assign parent $i^j = i$
STEP 4
Draw particles $\mathbf{x}_k^j$ ( $i=1, \dots, N$ ) from the prior density $\pi(\mathbf{x}_k \mathbf{x}_{k-1}^{i^j})$ , using the parent $i^j$ (particle index selected in the resampling of step 3), and then use the likelihood density to calculate the corresponding weights $w_k^j = \pi(\mathbf{z}_k^{obs} \mathbf{x}_k^j) / \pi(\mathbf{z}_k^{obs} \mu_k^{i^j})$ .
STEP 5
Normalize the particle weights so that $w_k^j = w_k^j / \sum_j w_k^j$ ( $j=1, \dots, N$ )

#### 4. DATA-DRIVEN WILDFIRE SPREAD USING PARTICLE FILTERS

In this paper, the SIR and ASIR algorithms are applied to natural fire propagation with the objective of accurately predicting the fire front position through the estimation of some physical parameters involved in the formulation of the Rothermel-based ROS in FIREFLY.

Data were taken from an experimental database corresponding to a small-scale (4 m x 4 m) open-field grassland fire occurring under moderate wind conditions [19],  $m_w = 1$  m/s blowing into a western direction ( $d_w = 307^\circ$ , in a clockwise representation where  $0^\circ$  indicates the North direction). The fire spread was recorded during 350 s using a thermal-infrared camera; the resulting observations are the time-evolving positions of the fire front (see Figure 4) identified as the contour lines where the temperature reaches the value 600 K, generally considered as the temperature of combustion ignition.

Details of the measurement technique to retrieve the temperature field from thermal imaging are given in Wooster et al. [29] and the subsequent reconstruction of the fire front positions is highlighted in Figure 4. In the following state estimation process, we assimilate measurements of fire front locations every 14 s from  $t = 64$  s to  $t = 106$  s (the associated fronts are represented in black solid lines in Figure 4). This means that, in the particle filters, the update step is successively performed at  $t = 64$  s, 78 s, 92 s and 106 s. This also means that the prediction step allows the PDF of the state variables and parameters to be integrated during 14 s between two consecutive observation times. Each observed front is discretely represented with  $N_f^o = 200$  markers, whose error standard deviation is estimated as 0.047 m (based on the spatial resolution of the thermal-infrared camera). This error standard deviation is used to describe the measurement covariance matrix  $\mathbf{W}$ .

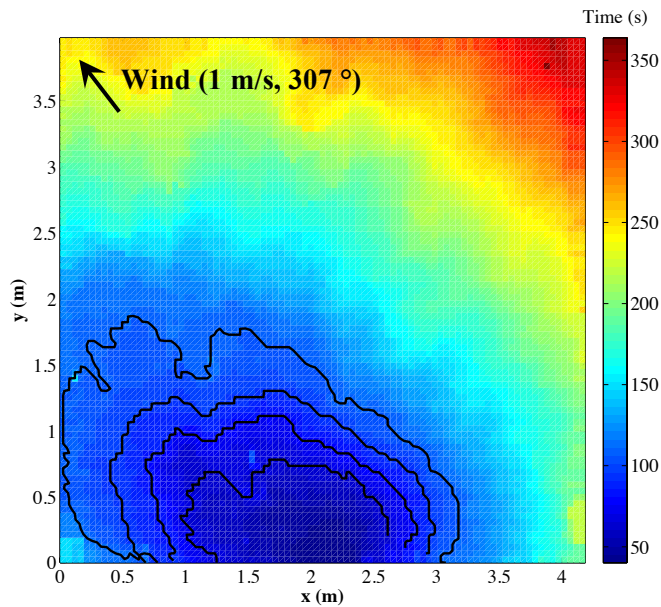


Figure 4: Arrival times of the fire front (in color) and observed fire fronts separated by 14 s (at  $t = 64$  s, 78 s, 92 s, 106 s) in black solid lines.

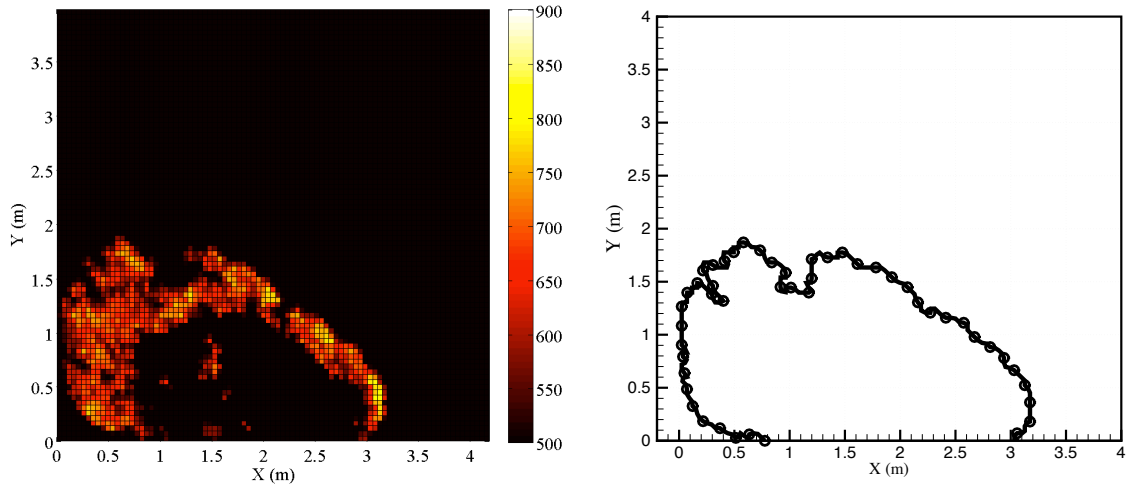


Figure 5: Extraction of the fire front location (right) from thermal-infrared imaging (left) at  $t = 106$  s; the fire front is identified as the 600-K temperature contour line.

The fire spread simulator assumes uniform properties of the (fuel) grass with a fuel layer thickness equal to  $\delta = 8$  cm (field measure), a fuel moisture content equal to  $M_f = 22$  % (field measure), and a fuel particle surface-to-volume ratio  $\Sigma = 11480$  1/m (values taken from Rothermel's database [2]). It is also assumed uniform and constant wind velocity magnitude and direction, respectively  $m_w = 1$  m/s and  $d_w = 307^\circ$ . Note that, even though the wind properties are constant, the local wind velocity vector  $\mathbf{u}_w$  along the normal direction to the fire front is modified by the deformation of the shape of the propagating fire front (see Section 2.1. for further explanations).

It was found in Rochoux et al. [19] that these values significantly underestimate the position of the fire fronts (the associated simulation, also called the free run in this paper, is shown in Figure 6) and that a state estimation procedure is therefore required to produce fire spread simulations that are more consistent with observations.

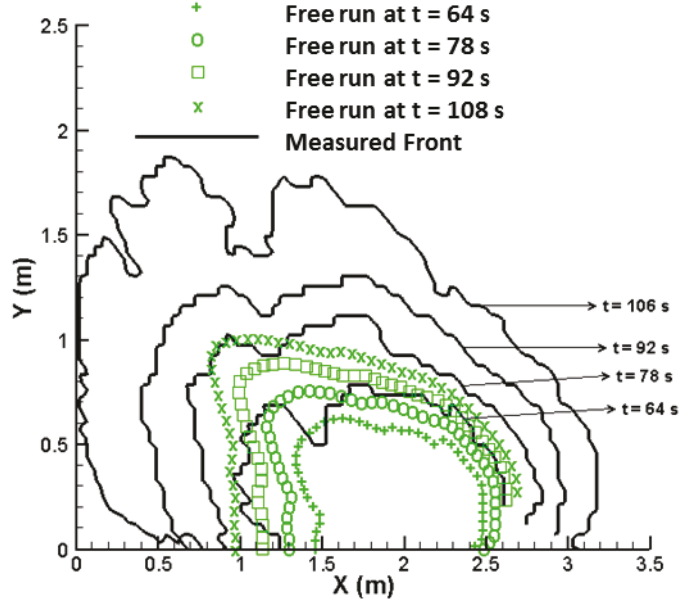


Figure 6: Comparison between the direct simulation (free run) and the measured fire front positions from  $t = 64$  s to  $t = 106$  s. Observations are represented in black solid lines, simulated fire fronts associated with the prior PDF of the control vector at  $t = 50$  s are represented in green symbols.

The objective of the present inverse problem is then to search for the posterior PDF of the fire front location. Due to their importance and inherent uncertainties, the fuel moisture content,  $M_f$ , and the fuel particle surface-to-volume ratio,  $\Sigma$ , are also treated as state variables in this work and estimated through the application of the particle filter algorithms under analysis. Their error standard deviations are taken to be 30 % of their initial mean values, that is  $\sigma_f = 6.6\%$  for  $M_f$  and  $\sigma_\Sigma = 3444$  1/m for  $\Sigma$ . The initial distributions of those variables for the particle filter algorithms were assumed as Gaussian, given as  $M_f = N(22\%, 6.6\%)$  and  $\Sigma = N(11480$  1/m, 3444 1/m). These two control parameters are assumed to be spatially-uniform. Note that no field measurement of the control parameters was performed during the controlled grassland fire experiment and that the validation of the results provided by the SIR and ASIR particle filters relies on the retrieval of the observed location of the fire front (the measurement error is small).

The 4 m x 4 m domain is discretized with a regular mesh ( $\Delta x = \Delta y = 0.047$  m), and the time step for integration of the progress variable equation is fixed to  $\Delta t = 0.02$  s. For each pair of control parameters taken in the associated Gaussian PDF, the fire spread simulation is initialized using the

corresponding initial state of the fire position at time  $t = 50$  s, and is then integrated in a time period of 14 s to update the posterior PDF of  $c$ ,  $M_f$  and  $\Sigma$ , at the 4 different observation times ( $t = 64$  s, 78 s, 92 s, 106 s). As there is no explicit formulation of the control vector evolution between 2 observation times, a random walk model is used; the error standard deviation introduced in the parameters from time  $t_{k-1}$  to time  $t_k$  is equal to  $\sigma_f$  for  $M_f$  and  $\sigma_\Sigma$  for  $\Sigma$ , respectively. It reads

$$M_f(t_k) = M_f(t_{k-1}) + \sigma_f R_f \quad (13)$$

$$\Sigma(t_k) = \Sigma(t_{k-1}) + \sigma_\Sigma R_\Sigma \quad (14)$$

with  $R_f$  and  $R_\Sigma$  random numbers following a Gaussian distribution, with zero mean and unitary standard deviation.

The state evolution model for the vector containing the values of the progress variable at each of the grid points,  $\mathbf{c}(t_k)$ , is obtained from the discrete integration of Equation (2) as described in Section 2.2. Uncertainties for  $\mathbf{c}(t_k)$  are assumed to be additive, Gaussian, with zero mean and a constant standard deviation of 0.01.

The performance of the SIR/ASIR particle filters is analyzed in the observation space, in terms of the Root Mean Square (RMS) error between the simulated and observed fire front positions, at each observation time. At time  $t_k$ , the RMS is calculated as follows:

$$RMS_k = \sqrt{\frac{1}{p} \sum_{j=1}^p (\mathbf{z}_{k,j}^{obs} - \mathbf{z}_{k,j})^2}, \quad (15)$$

where  $\mathbf{z}_k$  contains the  $p$  simulated fire front positions given by Equation (4), and  $\mathbf{z}_k^{obs}$  represents the corresponding observations. The 99%-confidence interval, denoted  $I_{99\%}$  and defined in the parameter space, is used as an additional diagnostic of the performance of the particle filters. It reads

$$I_{99\%} = \hat{\mathbf{x}}_k \pm 2.576 \boldsymbol{\sigma}_x, \quad (16)$$

where  $\hat{\mathbf{x}}_k$  represents the estimated mean value of the state variables and  $\boldsymbol{\sigma}_x$  represents its associated standard deviation.

The performance of both SIR and ASIR particle filters is presented in Table 4 in terms of RMS error at each observation/assimilation time and of the required computational time for the whole sequential Bayesian process, with different numbers of particles  $N$ . The different solutions of the

particle filters are also compared to the free run configuration (using standard Rothermel's database). Figures 7 and 8 present, along with the observations, the time-evolving location of the fire fronts (from  $t = 64$  s to  $t = 106$  s) estimated through the SIR and ASIR filters, respectively. These results show that both the SIR and ASIR filters are able to significantly reduce the distance between estimated and observed fire fronts and, thus, to closely track the observed fire fronts along time (see also Figure 6). The free run presents indeed the highest RMS errors for all observation times; the RMS errors for the SIR and ASIR filters are reduced by a factor of at least 2 for all observation times and in the best-case (i.e., at  $t = 92$  s) by a factor of 4, with respect to the free run RMS errors. Furthermore, these results indicate that the discrepancy to the observations remains significant at  $t = 106$  s due to the particular shape of the front, as shown in Figures 7 and 8. Note that here we do not have a spatial correction of the fire front position per observation time, as we assumed that the control parameters are spatially uniform and that tracking all the variations of the fire front topology at a given time was out of the scope of this study. Still, this representation is able to efficiently describe the propagation of the front in the wind direction and to accurately track the head of the fire, which is the main quantity of interest within an operational fire spread framework.

Table 4 also presents the computational time necessary to perform the inverse modeling process. The SIR algorithm with  $N$  particles requires the same computational time as the ASIR algorithm for  $N/2$  particles, due to the use of the characterization  $\mu_k$  to improve the prior information. For instance, the computational cost for the SIR algorithm with 100 particles is similar to that of the ASIR algorithm with 50 particles. Table 4 also shows that, even though the number of particles is increased to 400, the SIR algorithm does not succeed in converging towards a solution closer to the observations than with 50 particles, whereas the computational cost is multiplied by 25.

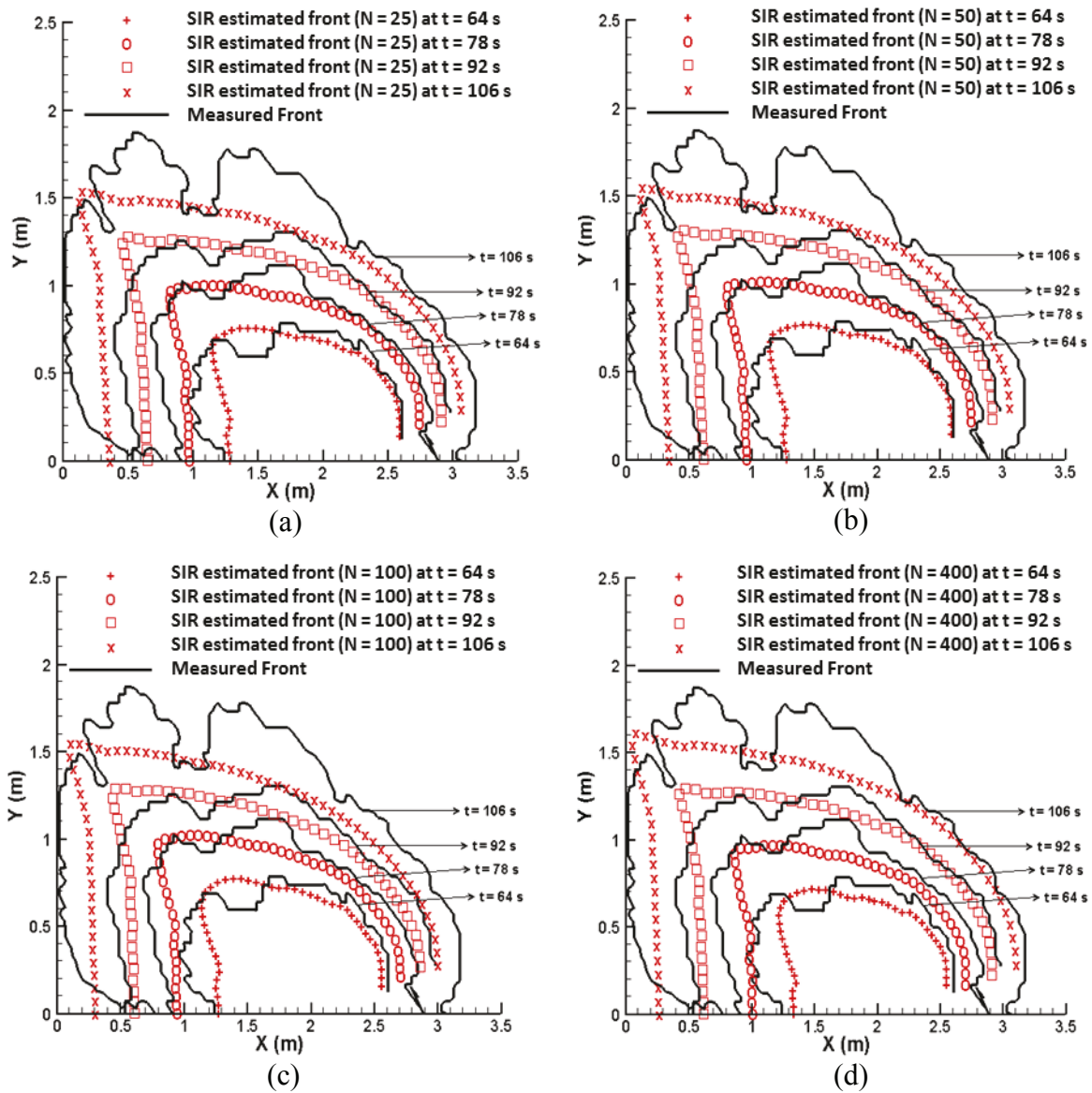


Figure 7: Comparison between simulated and measured fire front positions from  $t = 64$  s to  $t = 106$  s using the SIR filter, for: (a) 25 particles, (b) 50 particles, (c) 100 particles and (d) 400 particles. Observations are represented in black solid lines; simulated fire fronts associated with the posterior PDF of the control vector are represented in red symbols.

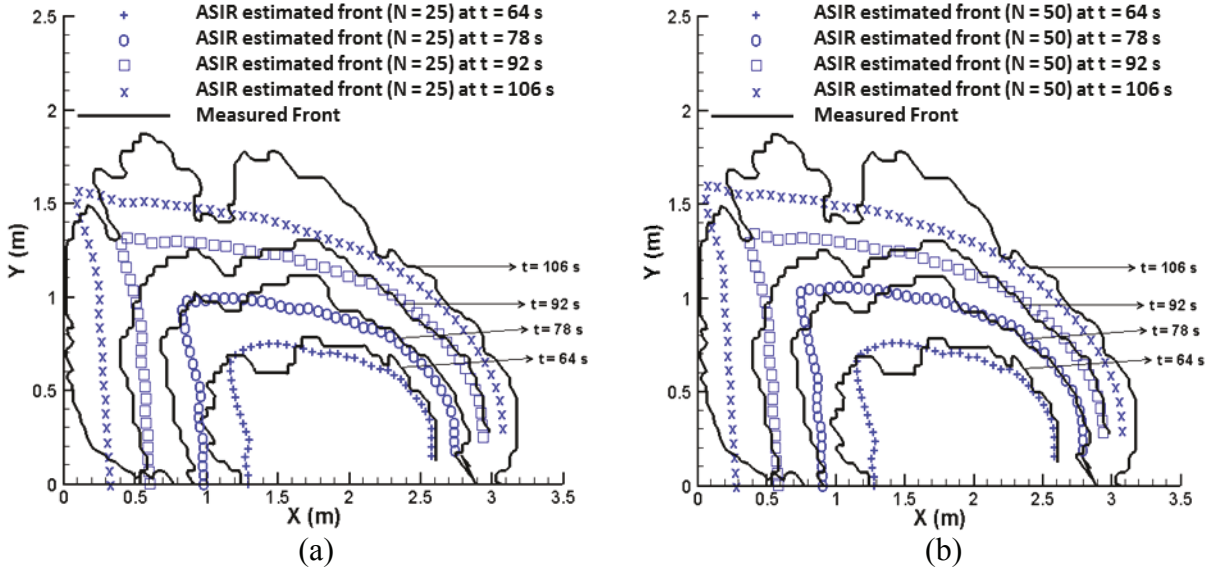


Figure 8: Comparison between simulated and measured fire front positions from  $t = 64$  s to  $t = 106$  s using the ASIR filter, for: (a) 25 particles, and (b) 50 particles. Observations are represented in black solid lines; simulated fire fronts associated with the posterior PDF of the control vector are represented in blue symbols.

Table 4. Computational times and RMS errors for SIR/ASIR filters.

Filter	Particle number ( $N$ )	RMS error ( $t = 64$ s)	RMS error ( $t = 78$ s)	RMS error ( $t = 92$ s)	RMS error ( $t = 106$ s)	CPU time (min)
Free run	-	0.3320 m	0.4062 m	0.4773 m	0.7629 m	1.639
SIR	25	0.1417 m	0.1915 m	0.1103 m	0.2900 m	9.0996
SIR	50	0.1418 m	0.1942 m	0.1107 m	0.2837 m	17.958
SIR	100	0.1378 m	0.2108 m	0.1194 m	0.2797 m	36.465
SIR	400	0.1791 m	0.2060 m	0.1105 m	0.2721 m	220.80
ASIR	25	0.1607 m	0.1952 m	0.1088 m	0.2826 m	17.987
ASIR	50	0.1461 m	0.1942 m	0.1212 m	0.2646 m	36.030

These results indicate that the application of the SIR and ASIR filter to the problem studied in this paper provides very similar values of the RMS errors between the mean and the measured values of the fire front position. It is therefore important to perform an analysis in the parameter space to further examine the performance of the SIR and ASIR filters. Figures 9 and 10 show, for both SIR and ASIR filters with different numbers of particles  $N$ , the mean values of the posterior distributions, along with their 99% confidence intervals  $I_{99\%}$ , associated with the fuel moisture content  $M_f$  and the fuel particle surface-to-volume ratio  $\Sigma$ , respectively. The posterior mean value found in Rochoux et al. [19] with

the EKF algorithm is also represented. It is found that the EKF solution is within the confidence interval and relatively close to the mean solution of the particle filters. Both data assimilation approaches provide consistent results, meaning that the EKF algorithm behaves reasonably well in this case, despite of its linearity assumption on the observation model. On the other hand, while the SIR filter with 100 particles is found to provide the mean of the posterior PDF that is the closest to the value given by the EKF, the ASIR filter with 50 particles provides a solution that reduces more effectively the width of the confidence interval for both parameters. This means that the ASIR filter with 50 particles provides a more reliable solution and thereby features a better approximation to the real fire spread than the SIR algorithm. Note that the prediction given by the particle filters is based on the mean value of the sought state variables and on their confidence intervals. Therefore, while the mean values are similar for these two filters for the problem studied in this paper, the confidence intervals are better predicted by the ASIR filter.

Figures 9 and 10, however, show that the width of the confidence interval remains relatively large for all examined cases. One factor that may affect the width of the confidence interval is the sample variability, meaning that several sets of control parameters may lead to the same simulated fire fronts close to the observations. The sample variability may be reduced if more sources of uncertainties such as the time-varying wind magnitude and direction are included in the Bayesian filtering procedure. Still, we note that the estimation of the pair of fuel parameters ( $M_f, \Sigma$ ) is sufficient to track extremely well the time-evolving observed fire spread. While the new values of the fuel moisture content  $M_f$  and the fuel particle surface-to-volume ratio  $\Sigma$  are realistic, they should be viewed as effective values that incorporate the effects of a number of modeling choices. However, errors may also come from other model input parameters (such as the wind magnitude and direction) or from the ROS model parameterization itself.

## 5. CONCLUSIONS

This paper has explored the capability of particle filters (also called sequential Monte Carlo approach) to improve the predictions of wildfire spread simulations using measurements of a reduced-scale controlled burning experiment. The proposed inverse modeling technique relied on the

estimation of a pair of parameters characterizing the properties of the grass vegetation. While both Sampling Importance Resampling (SIR) and Auxiliary Sampling Importance Resampling (ASIR) filters were able to sequentially track the displacement of the observed fire fronts, the ASIR filter allowed the retrieval of more accurate values of the control parameters (with a narrower confidence interval than the SIR filter) within a reasonable computational cost.

Ongoing research aims at further improving the Bayesian filtering strategy in order to better account for modeling uncertainties and to obtain more physical values of the control parameters. In this perspective, the control vector could incorporate more input parameters of the rate of spread model. However, the state estimation problem would require a larger set of particles to allow for the optimal posterior probability density function to be retrieved. This extension of the control vector seems feasible since surrogate models appear as promising approaches to limit the computational cost of Bayesian filtering problems based on Monte Carlo sampling, even if the physical problem becomes more complex. Ongoing research also aims at extensively evaluating the data-driven strategy against data from regional-scale wildfire spreads and not only on reduced-scale controlled fires. Due to the recent technological progress in geo-location of wildfires through airborne or spaceborne remote sensing, this evaluation becomes possible in the near future. Still, in this paper particle filters have already shown potential to relate comprehensively computational fire modeling and fire sensor technology, which is highly needed in the fire research area.

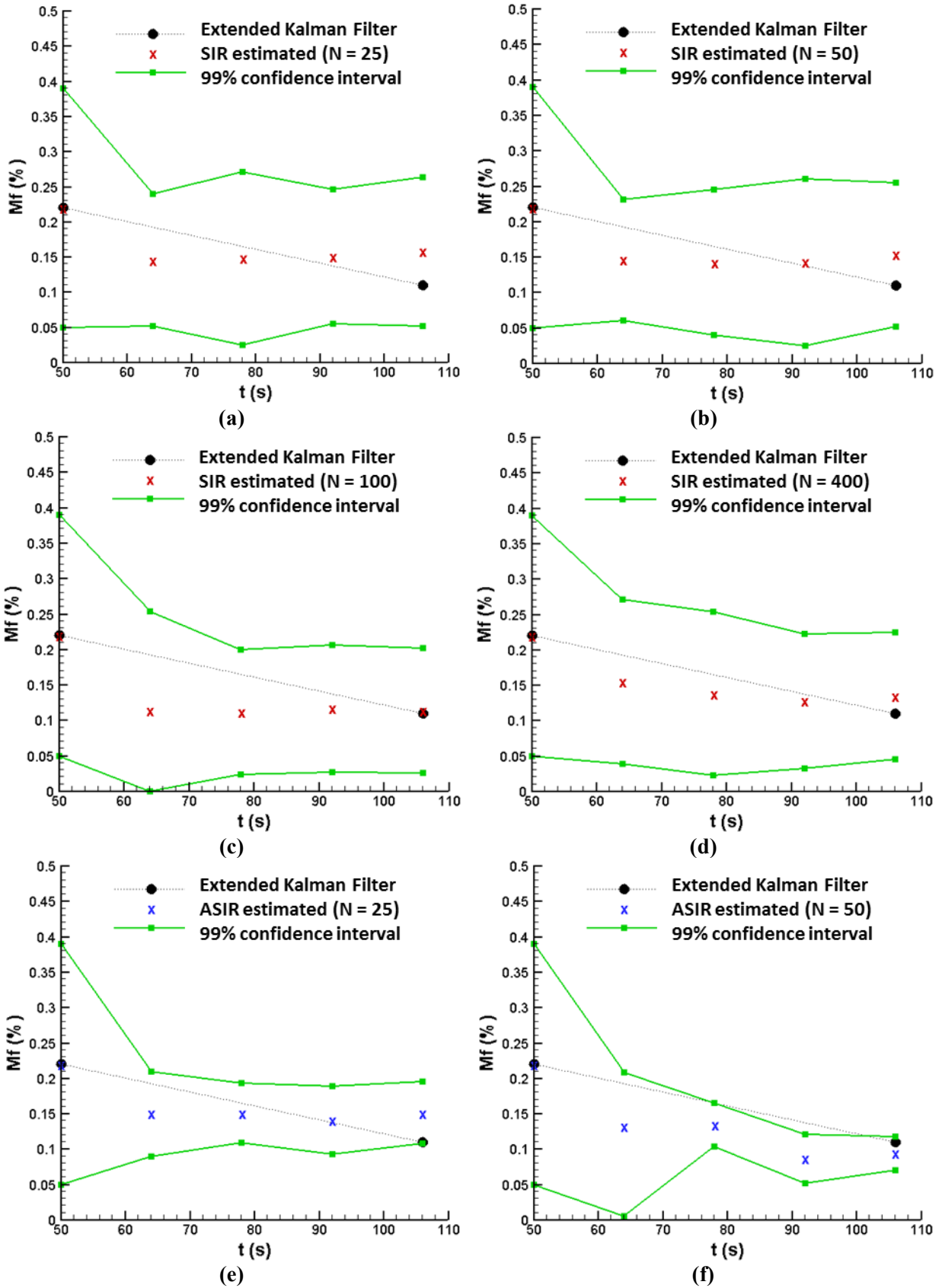


Figure 9: Sequential comparison of the estimation of the fuel moisture content  $M_f$  provided by the SIR/ASIR algorithm and the EKF [19]. Black plain dots represent the optimal solution for the EKF; colored crosses represent the mean value of the posterior PDF (red for the SIR filter, blue for the ASIR filter); and dotted solid lines represent the 99%-confidence interval  $I_{99\%}$ . (a) SIR filter with 25 particles, (b) SIR filter with 50 particles, (c) SIR filter with 100 particles, (d) SIR filter with 400 particles, (e) ASIR filter with 25 particles, (f) ASIR filter with 50 particles.

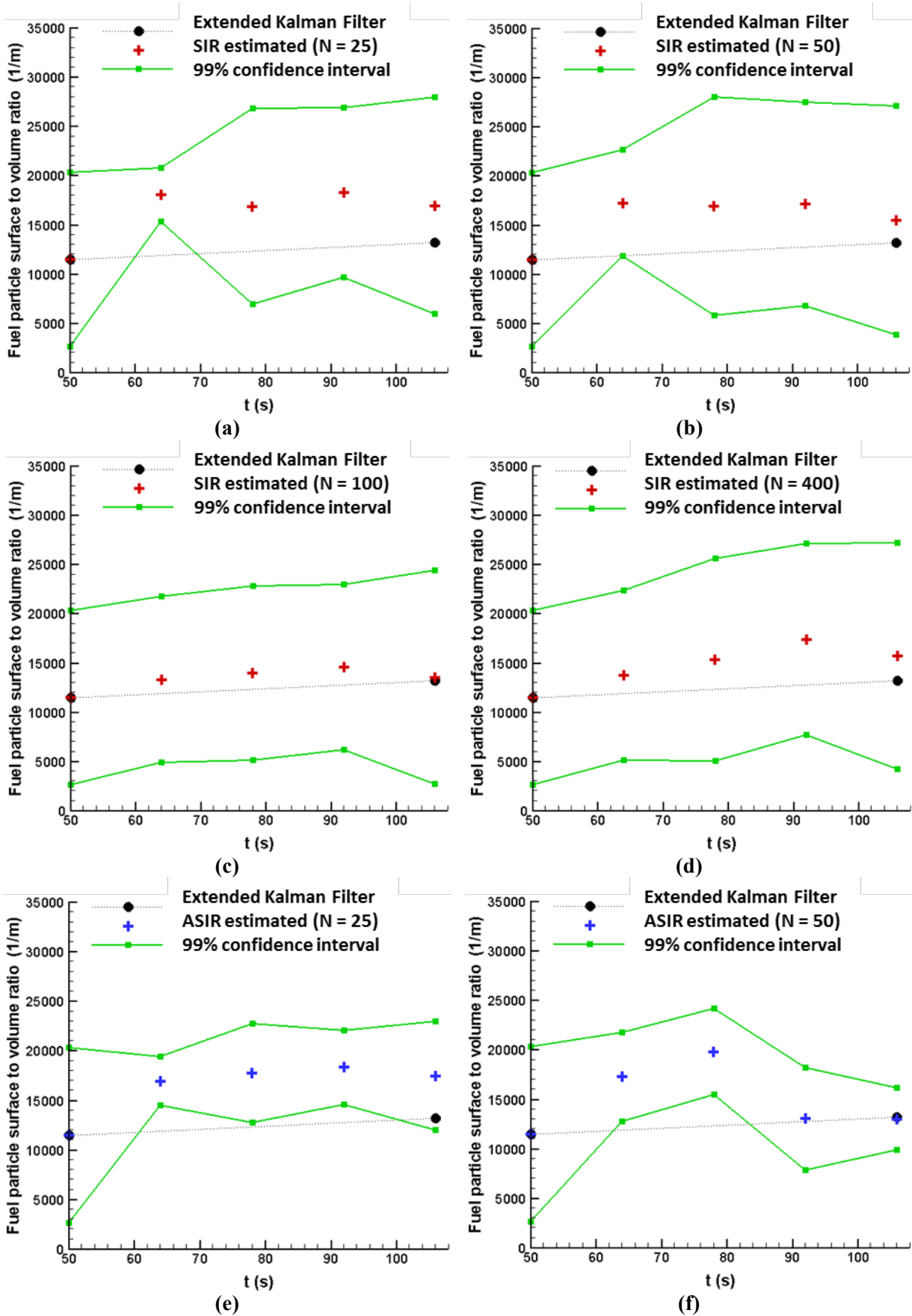


Figure 10: Sequential comparison of the estimation of the fuel particle surface-area-to-volume ratio  $\Sigma$  provided by the SIR/ASIR algorithm and the EKF [19]. Black plain dots represent the optimal solution for the EKF; colored crosses represent the mean value of the posterior PDF (red for the SIR filter, blue for the ASIR filter); and dotted solid lines represent the 99%-confidence interval  $I_{99\%}$ . (a) SIR filter with 25 particles, (b) SIR filter with 50 particles, (c) SIR filter with 100 particles, (d) SIR filter with 400 particles, (e) ASIR filter with 25 particles, (f) ASIR filter with 50 particles.

## 6. ACKNOWLEDGEMENTS

The financial support provided by FAPERJ, CAPES and CNPq, Brazilian agencies for the fostering of science, as well as the *Centre National pour la Recherche Scientifique* (CNRS) and the French ministry of foreign affairs (MAEE), is greatly appreciated. The authors also acknowledge the program STIC-AmSud for supporting the project «11STIC06-I3PE-Inverse Problems in Physical Property Estimation».

## 7. REFERENCES

- [1] Viegas, D.X., 2011, “Overview of Forest Fire Propagation Research”, *Proc. Intl. Assoc. Fire Safety Science*, 10, 95-108.
- [2] Rothermel, R.C., 1972, *A Mathematical Model for Predicting Fire Spread in Wildland Fuels*, Research Paper INT-115, US Department of Agriculture Forest Service.
- [3] Sullivan, A.L., 2009, “Wildland surface fire spread modeling, 1990-2007: 2. Empirical and quasi-empirical models”, *International Journal of Wildland Fire*, 18 (4), 369-386.
- [4] Gelb, A., 1974, *Applied Optimal Estimation*, Cambridge Massachusetts MIT Press.
- [5] Kaipio, J., Somersalo, E., 2004, *Statistical and Computational Inverse Problems*, Applied Mathematical Sciences 160, Springer-Verlag.
- [6] Kalman, R., 1960, “A New Approach to Linear Filtering and Prediction Problems”, *ASME J. Basic Engineering*, 82, 35-45.
- [7] Talagrand, O., 1997, “Assimilation of Observations, an Introduction”, *J. Meteor. Soc. Japan*, 75(1B), 191-209.
- [8] Doucet, A., Freitas, N., Gordon, N., 2001, *Sequential Monte Carlo Methods in Practice*, Springer, New York.
- [9] Ristic, B., Arulampalam, S., Gordon, N., 2004, *Beyond the Kalman Filter*, Artech House, Boston.
- [10] Gordon, N.J., Salmond, D.J., Smith, A.F.M., 1993, “Novel approach to non-linear/non-Gaussian Bayesian state estimation”, *Proceedings of IEEE*, 140(2), 107-113.

- [11] Orlande, H.R.B., Colaço, M.J., Dulikravich, G., Vianna, F., Silva, W.B., Fonseca, H., Fudym, O., 2012, "State Estimation Problems In Heat Transfer", *International Journal for Uncertainty Quantification*, 2(3), 239–258.
- [12] Pitt, M., Shephard, N., 1999, "Filtering via simulation: Auxiliary particle filters", *J. Amer. Statist. Assoc.*, 94(446), 590–599.
- [13] Silva, W.B., Orlande, H.R.B., Colaço, M. J., Fudym, O., "Application Of Bayesian Filters To A One-Dimensional Solidification Problem", *In: 21st Brazilian Congress of Mechanical Engineering*, Natal, RN, Brazil, 2011.
- [14] Colaço, M.J., Orlande, H.R.B., Silva, W.B., Dulikravich, G., "Application Of A Bayesian Filter To Estimate Unknown Heat Fluxes In A Natural Convection Problem", *Journal of Heat Transfer*, 134 (9), 092501.
- [15] Hamilton, F.C., Colaço, M.J., Carvalho, R.N., Leiroz, A.J.K., 2013, "Heat Transfer Coefficient Estimation of an Internal Combustion Engine Using Particle Filters", *Inverse Problems in Science and Engineering*, DOI:10.1080/17415977.2013.797411.
- [16] West, M., 1993, "Approximating posterior distributions by mixture", *J. R. Statist. Soc. B*, 55, 409–422.
- [17] Mandel, J., Bennethum, L.S., Beezley, J.D., Coen, J.L., Douglas, C.D., Kim, M., Vodacek, A., 2008, "A Wildland Fire Model With Data Assimilation", *Mathematics and Computers in Simulation*, 79, 584-606.
- [18] Gu, F., 2010, "Dynamic Data Driven Application System for Wildfire Spread Simulation", PhD thesis, Georgia State University.
- [19] Rochoux, M.C., Delmotte, B., Cuenot, B., Ricci, S., Trouvé, A., 2013, "Regional-Scale Simulations of Wildland Fire Spread informed by Real-time Flame Front Observations", *Proc. Combust. Inst.*, 34(2), 2641-2647.
- [20] Xue, H., Gu, F., Hu, X., 2012, "Data Assimilation Using Sequential Monte Carlo Methods in Wildfire Spread Simulation", *ACM Transactions on Modeling and Computer Simulation*, 22(4), 23:1-23:25.

- [21] Rochoux, M.C., 2014, “Vers une meilleure prévision de la propagation d’incendies de forêt : Evaluation de modèles et assimilation de données”, PhD thesis (in English), Ecole Centrale Paris.
- [22] Poinso, T., Veynante, D., 2005, *Theoretical and Numerical Combustion*, Second edition, R.T. Edwards.
- [23] Rehm, R.G., McDermott, R.J., 2009, “Fire front propagation using the level-set method”, NIST, Technical Report 1611.
- [24] Moradkhani, H., Hsu, K., Gupta, H., Sorooshian S., 2005, “Uncertainty Assessment of Hydrologic Model States and Parameters: Sequential Data Assimilation using Particle Filter”, *Water Resour. Res.*, 41, W05012, doi:10.1029/2004WR003604.
- [25] Desceliers, C., Ghanem, R., Soize, C., 2006, “Maximum likelihood estimation of stochastic chaos representations from experimental data”, *International Journal for Numerical Methods in Engineering*, 66(6), 978-1001.
- [26] Rochoux, M.C., Ricci, S., Lucor, D., Cuenot, B., Trouvé, A., Bart, J-M., 2012, “Towards predictive simulations of wildfire spread using a reduced-cost Ensemble Kalman Filter based on Polynomial Chaos approximations”, In *Proceedings of the Summer Program*, Center for turbulence Research, NASA AMES, Stanford University, USA, July 2012.
- [27] Orlande, H.R.B., Colaço, M.J., Dulikravich, G.S., 2008, “Approximation of the likelihood function in the Bayesian technique for the solution of inverse problems”, *Inverse Problems in Science & Engineering*, 16, 677-692.
- [28] Colaço, M.J., Dulikravich, G.S., Sahoo, D., 2008, “A Response Surface Method Based Hybrid Optimizer”, *Inverse Problems in Science & Engineering*, 16, 717-742.
- [29] Wooster, M.J., Roberts, G., Perry, G., Kaufman, Y.J., 2005, “Retrieval of biomass combustion rates and totals from fire radiative power observations: FRP derivation and calibration relationships between biomass consumption and fire radiative energy release”, *Journal of Geophysical Research*, 110, D2431.